Aromatic Hydrocarbon Nitration under Tropospheric and Combustion Conditions. A Theoretical Mechanistic Study

Giovanni Ghigo,[†] Mauro Causà,[‡] Andrea Maranzana,[†] and Glauco Tonachini*[,†]

Dipartimento di Chimica Generale ed Organica Applicata, Università di Torino, Corso Massimo D'Azeglio 48-10125 Torino, Italy, and Dipartimento di Scienze dell'Ambiente e della Vita DISAV, Università del Piemonte Orientale "Amedeo Avogadro", Corso Borsalino 54-15100 Alessandria, Italy

Received: July 14, 2006; In Final Form: October 6, 2006

The viability of some nitration pathways is explored for benzene (B), naphthalene (N), and in part pyrene (P). In principle, functionalization can either take place by direct nitration (NO_2 or N_2O_5 attack) or be initiated by more reactive species, as the nitrate and hydroxyl radicals. The direct attack of the NO_2 radical on B and N, followed by abstraction of the H geminal to the nitro group (most likely accomplished by $^3O_2$) could yield the final nitro-derivatives. Nevertheless, the initial step (NO_2 attack) involves significant free energy barriers. N_2O_5 proves to be an even worst nitrating agent. These results rule out direct nitration at room temperature. Instead, NO_3 and, even more easily, HO can form π-delocalized nitroxy- or hydroxycyclohexadienyl radicals. A subsequent NO_2 attack can produce several regio- and diastereoisomers of nitroxy-nitro or hydroxy-nitro cyclohexadienes. In this respect, the competition between NO_2 and O_2 is considered: the rate ratios are such to indicate that the NO_3 and HO initiated pathways are the major source of nitroarenes. Finally, if the two substituents are 1,2-trans, either a HNO_3 or a H_2O concerted elimination can give the nitro-derivatives. Whereas HNO_3 elimination is feasible, H_2O elimination presents, by contrast, a high barrier. Under combustion conditions the NO_2 direct nitration pathway is more feasible, but remains a minor channel.

Introduction

Aromatic compounds, in particular polycyclic aromatic hydrocarbons (PAHs) and their derivatives (PACs, polycyclic aromatic compounds), are ubiquitous species, introduced in the urban air by incomplete combustion processes. The presence of PACs is widespread, because they are produced from a variety of combustion sources, and they are known as primary and secondary tropospheric pollutants, especially in urban areas.[1−4] The oxidative pathways leading from PAHs to PACs can be characterized by the intervention of monomolecular steps, or by the involvement of other species, as HO, NO, NO_2, NO_3, or O_2, present in variable concentrations.[2,4,6] Different environmental or combustion conditions can thus modulate the relative importance of potentially competing pathways.

PAH oxidation processes produce a variety of compounds, which have been only partially identified.[4] Functionalization, which gives rise to PACs, can take place already during the combustion (PACs as primary pollutants), or at a later time, during the tropospheric transport of PAHs (PACs as secondary pollutants). PAHs and PACs share the same nature of soot,[7a] since both are generated in combustion processes at low O_2 concentrations. As the more or less disordered turbostratic[7b] graphenic layers grow, PAHs and PACs, due to their structural affinity, can be easily adsorbed on the forming fine soot particles. Thus, PAHs can be transported by the combustion-generated particulate, and their oxidation can be thought of as taking place not only in the gas phase but also in association with soot. PAHs and PACs can be conveyed by aerosol particles into the lungs, and be of concern as regards human health problems. In particular, some PAHs (for instance the intensively studied benzo[*a*]pyrene, BaP) are known to have carcinogenic and mutagenic properties. While transported, different PAHs decay at very different rates. Then, the relative amount of carcinogenic/mutagenic primary products changes significantly, and other products form, whose nature is in some cases known, while in others it is not. The functionalization of PAHs (and of soot itself) has been studied by both field campaigns and laboratory studies.[8]

Among the possible functionalized products, the nitroarenes, whose formation is the subject of the present study, appear to be particularly interesting, since some of them are dangerous mutagenic and carcinogenic compounds.[9] These compounds (which have been detected as important trace pollutants in urban areas)[10−12] can originate, as seen, in the urban air as the outcome of incomplete combustion (e.g., 1-nitropyrene is a primary pollutant in diesel exhaust), but can also be produced as secondary pollutants by way of tropospheric processes. Having been detected in diesel exhaust, they have also been supposed to originate on the surface of particulate matter.[13] The formation of nitroarenes has also been the subject of laboratory studies, both in the gas phase[14] and in association with solid surfaces.[6]

Useful mechanistic information on this point is also expected from a theoretical investigation, which will result complementary to the collection of experimental results accumulated as yet. Our foregoing theoretical studies on (i) the initial steps of the oxidative degradation of benzene[16] and (ii) the subsequent steps leading to aldehydes and aldehyde epoxides[17−19] were intended as such a contribution. In particular, few theoretical studies on nitroaromatics have appeared in recent years. These papers deal either with nitroresorcinols, whose conformational structures and energies have been investigated by DFT(B3LYP) computations,[20a]

* Address correspondence to this author. E-mail: glauco.tonachini@unito.it. Fax: 39-011-2367648. Web site: http://thecream.unito.it.

[†] Università di Torino.

[‡] Università del Piemonte Orientale

10.1021/jp064459c CCC: $33.50
Published on Web 11/21/2006

TABLE 1: Initial Radical Attacks Which Could Open the Way to Benzene (B) Nitration

		$\Delta E^{a,b}$	ΔH^b $T = 298$ K	ΔG^b $T = 298$ K	ΔG^b $T = 1200$ K
reaction **1**: **B** + NO_2		0.0	0.0	0.0	0.0
addition TS		19.9	20.1	29.5	56.3
nitrocyclohexadienyl radical	**B-I**	19.4	20.5	29.1[c]	55.9
reaction **2**: **B** + NO_3		0.0	0.0	0.0	0.0
addition TS		3.6	5.3	16.7	50.5
nitroxycyclohexadienyl radical	**B-II**	−0.6	1.7	13.2	46.3
reaction **3**: **B** + $HO^{\bullet}$		0.0	0.0	0.0	0.0
addition TS		−3.1	−2.3	5.4	32.1
hydroxycyclohexadienyl radical	**B-III**	−17.7	−15.5	−7.2	17.1
reaction **4**: **B** + N_2O_5		0.0	0.0	0.0	0.0
syn−1,2-addition TS		29.1	28.5	38.6	66.6
H-transfer/addition TS		27.5	27.2	38.3	70.3

[a] From corrected DFT(B3LYP)/6-311+(2df,p)//6-31G(d) energy values. [b] Units: kcal mol^{-1}; $T = 298$ K. [c] Value for the minimum of a complete free energy profile: *G* computed at the *E* minimum geometry gives a *G* value 0.5 kcal mol^{-1} higher than the TS G.

TABLE 2: Initial Attacks Which Can in Principle Open the Way to Naphthalene (N) Nitration

		$\Delta E^{a,b}$	ΔH^b $T = 298$ K	ΔG^b $T = 298$ K	ΔG^b $T = 1200$ K
reaction **1**: **N** + NO_2		0.0	0.0	0.0	0.0
TS for addition in 1		13.8	14.3	25.2	57.2
1-nitrobenzocyclohexadienyl radical	**1-N-I**	12.5	14.0	25.2	56.7
TS for addition in 2		17.1	17.5	28.5	60.2
2-nitrobenzocyclohexadienyl radical	**2-N-I**	16.4	17.7	28.7	59.5
reaction **2**: **N** + NO_3		0.0	0.0	0.0	0.0
TS for addition in 1		−3.0	−1.0	11.8	50.1
1-nitroxybenzocyclohexadienyl radical	**1-N-II**	−8.2	−5.6	7.5	45.5
TS for addition in 2		0.4	2.3	15.1	53.4
2-nitroxybenzocyclohexadienyl radical	**2-N-II**	−3.5	−1.0	12.0	52.0
reaction **3**: **N** + $HO^{\bullet}$		0.0	0.0	0.0	0.0
TS for addition in 1		−5.4	−4.6	4.4	32.0
1-hydroxybenzocyclohexadienyl radical	**1-N-III**	−24.9	−22.5	−12.7	16.0
TS for addition in 2		−4.3	−3.4	5.7	34.7
2-hydroxybenzocyclohexadienyl radical	**2-N-III**	−20.4	−18.1	−8.4	20.4
reaction **4**: **N** + N_2O_5		0.0	0.0	0.0	0.0
TS for H-transfer and addition in 1		23.6	23.6	36.1	72.4

[a] From corrected DFT(B3LYP)/6-311+(2df,p)//6-31G(d) energy values. [b] Units: kcal mol^{-1}.

or with large amino or nitroaromatics, studied by low-level DFT-(Xα) calculations.[20b] A very recent paper deals with the NO_3-promoted gas-phase nitration of phenol and toluene.[20c] Reactivity studies (in which transition structures and reaction intermediates are defined, and reaction pathways compared) are still apparently rare. Our present theoretical research aims to fill, at least partially, the existing gap between the mentioned lack of theoretical data and the available experimental literature. It is articulated along two lines. The first one (to which this paper belongs) aims to elucidate the gas-phase oxidation and functionalization mechanisms of aromatics. The second one has the purpose of defining a suitable model for soot,[21,22] and investigating the interaction of small molecular species (as HO, NO, NO_2, O_3 or O_2, etc.) and of aromatics with it. Both projects converge on elucidating the possible role of soot in setting the scenario for the possible functionalization channels of aromatic compounds.

Methods

The stable and transition structures (TS) were determined by gradient procedures[23] within the Density Functional Theory (DFT), and making use of the B3LYP functional.[24] This functional is of widespread use, and, even if prone to underestimate some reaction barriers, has generally performed well as regards geometries and energetics.[25] The polarized 6-31G(d) basis set[26] was used in the DFT(B3LYP) optimizations. Then the nature of the critical points was checked by diagonalization of the 6-31G(d) analytic Hessian (vibrational analysis). A limited set of single-point energy calculations, carried out with four different basis sets on the 6-31G(d) structures, were compared with a 6-311+G(3df,2p)//6-31G(d) energy calculation to find out the better compromise between their dependability and computational feasibility (see the Supporting Information). The 6-311+G(2df,p) basis set[26] was then chosen for all the final single-point energy calculations. The energy values so obtained were refined by getting rid of the contamination due to the next higher spin multiplicity of the same parity, by using Yamaguchi's formula.[27] These final "corrected" DFT(B3LYP)/6-311+G(2df,p)//6-31G(d) energies were then combined with the 6-31G(d) thermochemical corrections from the vibrational analysis to get estimates of the activation and reaction enthalpies and free energies.[28] The relevant enthalpy and free energy differences are collected in Tables 1−5. A more complete set of energies, enthalpies, and free energies is presented (together with the relevant critical point geometries) in the Supporting Information.

To assess an estimate to the free energy barriers the following procedure was adopted. When a single interatomic distance *R* characterizes the reaction profile, as in bimolecular adduct formations, a series of constrained optimizations on the reacting system were carried out in proximity of the TS geometry. The energy was minimized in correspondence of fixed *R* values, smaller and larger with respect to its value in the TS. Otherwise, as in the concerted H transfer between two atoms, the intrinsic reaction coordinate (IRC)[29] was defined, starting from the TS geometry on the *E* surface. For each point generated along the profile by any of the two methods, *G* was estimated by carrying

TABLE 3: Steps from the Cyclohexadienyl Radicals to Nitrobenzene

		$\Delta E^{a,b}$	ΔH^b $T = 298$ K	ΔG^b $T = 298$ K	ΔG^b $T = 1200$ K
reaction **5**:					
nitrocyclohexadienyl radical + O_2	**B-I** + O_2	0.0	0.0	0.0	0.0
TS for H transfer to O_2		7.1	4.9	14.5	41.2
O_2 addition TS		5.7	6.7	19.1	53.2
trans-1-nitro−2-peroxyl adduct	**B-IV**	−1.8	0.8	12.1	45.0
HOO elimination TS		4.0	3.6	15.9	52.1
nitrobenzene + HOO	**B-V** + HOO•	−15.6	−14.6	−14.4	−13.5
nitroxycyclohexadienyl radical + NO_2	**B-II** + NO_2	0.0	0.0	0.0	0.0
reaction **6**: NO_2 addition "TS" [c]		-	-	7.8	47.8
reaction **7**: *O_2 addition TS* [d]		*6.0*	*7.0*	*19.1*	*52.4*
trans−1-nitroxy-2-peroxyl adduct [d]	*trans*-**1,2-B-IV**	*−2.7*	*0.0*	*11.0*	*42.7*
TS HOO elimination (*i*) [d]		*3.6*	*2.9*	*14.3*	*47.6*
ring closure TS (*ii*)[d]		*13.0*	*14.6*	*27.5*	*66.2*
trans-1-nitroxy−2-nitro adduct	*trans*-**1,2-B-VI**	−26.8	−22.9	−10.1	27.6
HNO_3 elimination TS		−6.6	−5.3	7.2	62.1
nitrobenzene + HNO_3	**B-V** + HNO_3	−57.3	−58.0	−51.3	−49.8
hydroxycyclohexadienyl radical + NO_2	**B-III** + NO_2	0.0	0.0	0.0	0.0
reaction **8**: NO_2 addition "TS" [c]		-	-	7.6	40.0
reaction **9**: *O_2 addition TS* [d]		*4.4*	*5.4*	*17.6*	*52.3*
reaction **9**: *TS for direct H abstraction*		*4.4*	*3.0*	*13.0*	*41.9*
trans-1-hydroxy−2-nitro adduct	*trans*-**1,2-B-VII**	−27.9	−24.0	−11.2	26.8
H_2O elimination TS		13.3	12.8	26.6	67.0
nitrobenzene + H_2O	**B-V** + H_2O	−57.3	−55.7	−53.4	−48.2

[a] From corrected DFT(B3LYP)/6-311+(2df,p)//6-31G(d) energy values. [b] Units: kcal mol^{-1}. [c] Maximum along a *G* profile generated in correspondence of an all-downhill *E* profile (see text). [d] Referred to a **B-II** or **B-III** + O_2 energy or free energy zero; the maxima for O_2 addition are determined as described in the main text (in the case of dioxygen a TS on the energy surface is present).

TABLE 4: Steps from the 1-X-benzocyclohexadienyl Radicals (X = Nitroxy, Hydroxy) to 2-Nitronaphthalene

		$\Delta E^{a,b}$	ΔH^b $T = 298$ K	ΔG^b $T = 298$ K	ΔG^b $= 1200$ K
1-nitroxycyclohexadienyl radical + NO_2	**1-N-II** + NO_2	0.0	0.0	0.0	0.0
NO_2 addition "TS"[c]				7.6	41.4
O_2 addition TS[d]		*3.4*	*4.4*	*16.5*	*49.6*
trans-1-nitroxy-2-peroxyl adduct[d]		*−5.6*	*−3.0*	*7.9*	*39.2*
TS HOO elimination (*i*)[d]		*4.8*	*3.6*	*14.9*	*48.0*
ring closure TS (*ii*)[d]		*19.0*	*20.2*	*31.9*	*66.9*
TS for direct H abstraction[d]		*8.1*	*6.0*	*16.1*	*44.7*
trans-1-nitroxy−2-nitro adduct	*trans*-**1,2-N-VI**	−29.2	−25.4	−12.8	24.4
HNO_3 elimination TS		−7.5	−6.7	6.1	44.4
2-nitronaphthalene + HNO_3	**2-V** + HNO_3	−50.1	−47.8	−46.9	−43.4
1-hydroxycyclohexadienyl radical + NO_2	**1-N-III** + NO_2	0.0	0.0	0.0	0.0
NO_2 addition "TS"[c]				7.7	39.1
O_2 addition TS[d]		*1.7*	*2.6*	*14.7*	*47.4*
trans-1-hydroxy-2-peroxyl adduct[d]		*−7.1*	*−4.6*	*6.6*	*39.3*
TS HOO elimination (*i*)[d]		*1.5*	*2.1*	*13.0*	*40.5*
2,3-ring closure TS (*ii*)[d]		*19.8*	*20.9*	*32.7*	*67.9*
2,4-ring closure TS (*ii*)[d]		*27.0*	*27.7*	*40.2*	
TS for direct H abstraction[d]		*6.3*	*4.4*	*14.9*	*45.3*
trans-1-hydroxy−2-nitro adduct	*trans*-**1,2-N−VII**	−31.6	−27.8	−15.2	22.0
H_2O elimination TS		13.5	12.9	26.7	67.5
2-nitronaphthalene + H_2O	**2-N-V** + H_2O	−50.4	−49.2	−46.7	−41.5

[a] From corrected DFT(B3LYP)/6-311+(2df,p)//6-31G(d) energy values. [b] Units: kcal mol^{-1}. [c] Maximum along a *G* profile generated in correspondence of an all-downhill *E* profile. [d] The maxima for O_2 addition are determined as described in the main text, and are referred to an energy or free energy zero defined by **N-II** or **N-III** + O_2 (in the case of dioxygen a TS on the energy surface is present).

out a vibrational analysis and projecting out the imaginary frequency related to the reaction coordinate.[30] The maximum along the *G* profile so obtained defined the best estimate of the *G* barrier height. This time-consuming procedure was not adopted when the process at hand was very unfavorable or not too interesting, as in the dinitrogen pentoxide additions and in the water elimination step (*G* computed at the geometry of the transition structure on the *E* hypersurface).

These calculations were carried out by using the GAUSSIAN 03 system of programs.[31]

In addition, the first reaction step for each benzene pathway (attacks of X = NO_2, NO_3, and HO) was inspected by using the composite method CBS-Q//B3.[32] Similarly, the attack of X on ethene was studied. Also the G3-RAD[33] method was used, but limited to the HO attack on benzene. Unfortunately, these computations turn out not to be feasible, neither on the larger systems (naphthalene + X) nor for the further steps which involve the benzene-X adduct + O_2. The CBS-Q//B3 calculations were carried out by again using GAUSSIAN 03, while the G3-RAD computations were done with the ACES II program.[34]

Results and Discussion

Initial Attacks by Radical Species. *Benzene*. The attacks of the NO_2, NO_3, or HO radicals on the aromatic ring of benzene

TABLE 5: Steps from the 1-Nitro- and 2-X-benzocyclohexadienyl Radicals (X = Nitroxy, Hydroxy) to 1-Nitronaphthalene

		$\Delta E^{a,b}$	ΔH^b $T = 298$ K	ΔG^b $T = 298$ K	ΔG^b $T = 1200$ K
1-nitrocyclohexadienyl radical + O_2	**1-N-I** + O_2	0.0	0.0	0.0	0.0
TS for H transfer to O_2		10.8	8.7	19.3	49.6
O_2 addition TS		3.0	3.9	15.8	49.1
trans-1-nitro−2-peroxyl adduct	**1-N-IV**	−4.9	−2.4	9.4	43.5
HOO elimination TS		7.2	6.1	18.5	54.0
1-nitronaphthalene + HOO•	**1-N-V** + HOO	−4.5	−3.9	−4.0	−4.3
2-nitroxycyclohexadienyl radical + NO_2	**2-N-II** + NO_2	0.0	0.0	0.0	0.0
NO_2 addition "TS"[c]				7.6	36.9
O_2 addition TS[d]		*−2.0*	*−1.3*	*10.1*	*41.9*
trans-2-nitroxy−1-peroxyl adduct[d]			*−8.4*	*2.8*	*33.8*
TS HOO elimination (i)[d]		*1.1*	*−0.1*	*11.4*	*42.7*
ring closure TS (ii)[d]		*7.6*	*9.2*	*21.9*	*58.2*
trans-1-nitro-2-nitroxy adduct	*trans*-**1,2-N-VI**		−29.3	−16.0	20.9
HNO_3 elimination TS		−10.7	−9.5	3.4	40.0
1-nitronaphthalene + HNO_3	**1-N-V** + HNO_3	−50.3	−47.8	−46.9	−45.3
2-hydroxycyclohexadienyl radical + NO_2	**2-N-III** + NO_2	0.0	0.0	0.0	0.0
trans-1-nitro-2-hydroxy adduct[e]	*trans*-**1,2-N-VII**		−32.2	−19.5	20.2
H_2O elimination TS[e]		12.9	12.5	26.1	66.5
1-nitronaphthalene + H_2O	**1-N-V** + H_2O		−48.9	−46.5	−41.4

[a] From corrected DFT(B3LYP)/6-311+(2df,p)//6-31G(d) energy values. [b] Units: kcal mol^{-1}. [c] Maximum along a *G* profile generated in correspondence of an all-downhill *E* profile. [d] The maxima for O_2 addition are determined as described in the main text, and are referred to a **N-II** or **N-III** + O_2 energy or free energy zero (in the case of dioxygen a TS on the energy surface is present). [e] Given the unpromising water elimination step defined for the other position (NO_2 addition in 1, HO in 2; see Table 5), the maximum along the *G* profile was not looked at for the NO_2 addition and the H_2O elimination. In this second case, *G* was computed at the TS geometry.

SCHEME 1

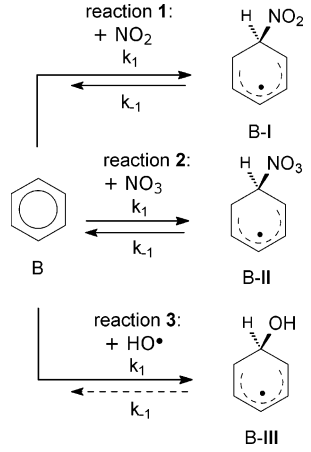

(**B**) were first considered (Scheme 1 and Table 1: reactions 1−3, respectively), and their possible competition assessed. Dinitrogen pentoxide was also considered (reaction 4).

NO_2 addition, which leads to the nitrocyclohexadienyl radical adduct (**B-I**), is definitely endothermic, and the unfavorable entropy term makes it even more demanding in terms of free energy ($\Delta G = 29$ kcal mol^{-1}, at $T = 298.15$ K, 298 for short in the following). The second one produces the nitroxycyclohexadienyl radical intermediate (**B-II**) in a still endothermic and endoergic step ($\Delta G = 13$ kcal mol^{-1}). By contrast, the third process, which produces the hydroxycyclohexadienyl radical intermediate (**B-III**), is exothermic enough that the enthalpy change prevails on the entropy contribution, resulting in $\Delta G = -7$ kcal mol^{-1}. The relevant free energy barriers drop off correspondingly, in the following sequence: 29 (NO_2), 17 (NO_3), and 5 (HO) kcal mol^{-1} (at $T = 298$ K). The straightforward estimate of the free energy barrier height in correspondence of the TS geometry is verified by means of a couple of constrained optimizations at shorter and larger C−N or C−O distances. This confirms the geometrical location of the maximum along the G profile in correspondence of the TS on the *E* surface, and yields the values reported in Table 1. In all cases, the entropy term is appreciably adverse, and contributes to raise the barrier, with respect to the enthalpy difference values, by 8−11 kcal mol^{-1}, at room temperature (Supporting Information).

At $T = 298$ K, rate constant ratios are very adverse to direct nitration. They can be roughly estimated on the basis of Table 1 (just as k_1 for the forward step in Scheme 1), as $k_{NO_2}/k_{NO_3} \approx 5 \times 10^{-10}$ and $k_{NO_2}/k_{HO} \approx 3 \times 10^{-18}$ ($T = 298$ K). The rate for the NO_2 attack relative to those for NO_3 and HO can be reckoned by setting $[NO_3] = 2 \times 10^8$ molecules cm^{-3} (12-h nighttime average concentration) and $[HO] = 1.5 \times 10^6$ molecules cm^{-3} (12-h daytime average concentration);[35a] $[NO_2]$ can even be set to 10^{12} molecules cm^{-3}, to simulate an extremely polluted situation and put its pathway on a favorable ground. Nevertheless, the estimated ratios oppose the direct nitration in any case: $v_{NO_2}/v_{NO_3} \approx 10^{-6}$ and $v_{NO_2}/v_{HO} \approx 10^{-12}$. Moreover, while the ΔG data for the backward processes indicate that the hydroxycyclohexadienyl radical intermediate **B-III** will be less inclined toward decomposition back to the reactants than the analogous nitroxy intermediate **B-II**, the tiny barrier estimated for nitro adduct **B-I** casts some doubts on its very existence.

Under combustion conditions, say at 1200 K, the assessment of the free energy profiles provides much higher barriers and, consistently, maxima located at shorter intermolecular distances (a later "TS", in a geometrical sense). The *G* profiles have to be redefined at the higher temperature by performing the vibrational analysis as already described. The barrier height is 56 kcal mol^{-1} for NO_2 and the maximum occurs at $R = 1.74$ Å (vs 1.79 at 298 K). For HO it is 32 kcal mol^{-1} ($R = 1.93$ Å, vs 2.03 at 298 K). The NO_3 data in Table 1 are reported for completeness, but under these conditions its concentration should be ineffective. The attack by NO_2 is more difficult than that by HO by ca. 24 kcal mol^{-1}, which gives a small rate constant ratio $k_{NO_2}/k_{HO} \approx 4 \times 10^{-5}$, though significantly higher than that at room temperature. This datum hardly can be compensated by the concentration factor. In fact, even if $[NO_2]$ is set to 10^{13} molecules cm^{-3},[35b] [HO] can also be quite high under these conditions,[35c] even higher than $[NO_2]$. The hypothetical rate ratio would be in favor of the HO attack under most combustion

SCHEME 2: Transition Structures for Two Attacks to Benzene by N_2O_5 (Reaction 4)

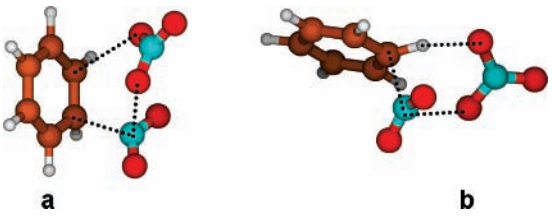

conditions. Moreover, it can be seen from Table 1 that the reverse process (dissociation to reactants) is again easier for the nitrocyclohexadienyl radical adduct **B-I** than for the hydroxy intermediate **B-III**.

N_2O_5 is a possible nitrating agent, formed during the night by the reaction of NO_3 with NO_2. It had been studied as a nitrating agent in some experimental studies on naphthalene (in the gas phase),[36,37] pyrene, perylene,[38] and other PAHs[39] (adsorbed on glass fiber filters or on atmospheric soot particles).[40] In the present study, the efficiency of nitrogen pentoxide as a gas-phase nitrating agent was explored for benzene and position 1 of naphthalene (reaction 4). Its attack can be concerted to different extents. It either implies, as a first step, the *syn*-1,2-addition of the still partially connected NO_3 and NO_2 moieties (Scheme 2a), or NO_3 abstracts a hydrogen atom from benzene, while NO_2 adds to the same carbon atom that undergoes the H abstraction (Scheme 2b). In benzene, the first attack would yield a *syn*-1-nitroxy-2-nitro cyclohexadiene intermediate, while the second one would directly give nitrobenzene and HNO_3. However, both reactions require the overcoming of very high barriers, corresponding (at $T = 298$ K) to $\Delta G^{\ddagger} \approx 38$ kcal mol^{-1}, for both the 2a and 2b attacks (see the Supporting Information). Such a result seems to rule out the importance of N_2O_5 as a gas-phase nitrating agent, at least for benzene.

Performance of DFT and Composite Methods. The results just described, obtained for the first step of each benzene pathway (attacks of X = NO_2, NO_3, and HO, labeled as reactions 1, 2, and 3 in Scheme 1), were compared to those provided by the composite method CBS-Q//B3.[32] For the HO attack on benzene, the G3-RAD[33] method was used also. For the first two additions, the spin-corrected CBS-Q//B3 estimate of the barrier is lower than that from DFT(B3LYP). The CBS-Q//B3 barrier for NO_2 is $\Delta G^{\ddagger} = 26.0$ kcal mol^{-1}, to be compared with 29.5 kcal mol^{-1} from DFT(B3LYP). If, however, the spin correction is not applied, as suggested by Radom et al.,[33b] the U-CBS-Q//B3 (U = uncorrected) barrier for NO_2 becomes $\Delta G^{\ddagger} = 28.6$ kcal mol^{-1}, in closer agreement with the DFT estimate. A similar result is presented by this composite method for the addition of NO_3 to benzene. The CBS-Q//B3 barrier is only $\Delta G^{\ddagger} = 10.4$ kcal mol^{-1}, which compares with 16.7 kcal mol^{-1} from DFT(B3LYP), but the uncorrected barrier rises to 13.1 kcal mol^{-1}, again in better agreement with the DFT value.

The addition of HO to benzene has a CBS-Q//B3 barrier $\Delta G^{\ddagger} = 4.3$ kcal mol^{-1}, not far from the 5.4 kcal mol^{-1} estimate of DFT(B3LYP). In sharp (and disturbing) contrast with the preceding results, the barrier rises, however, as high as 11.1 kcal mol^{-1} if the spin correction is omitted. Radom's G3-RAD composite method,[33a] which relies on an initial ROHF computation and does not need, consequently, any spin-correcting procedure, gives in turn an estimate of $\Delta G^{\ddagger} = 7.6$ kcal mol^{-1}. Figure 1 summarizes these results, which unfortunately could not be extended any further.[41a] We can also mention a recent computational result on the HO + benzene reaction, in which the gas-phase DFT(B3LYP)/6-311+G(d,p)//DFT(B3LYP)/6-31+G(d,p) free energy addition barrier at 298 K is reported to be 7.4 (6.7 with the 6-31G(d) basis set) kcal mol^{-1} high[41b] (whereas in less recent papers the addition of HO to methylated benzenes had been investigated theoretically).[41c]

In addition, two experimental rate constant measurements can be reported. The first one[42] is relevant to the addition of hydroxyl to benzene, and the rate constant is assessed in the range $k = 1.1 \times 10^{-12}$ to 7.3×10^{-12} s^{-1} molecule^{-1} cm^3. These values translate into $\Delta G^{\ddagger} = 4.3-5.4$ kcal mol^{-1} (this range compares well with both CBS-Q//B3 and DFT results). The second one is an estimate for the addition of the nitrate radical to benzene: $k < 1.5 \times 10^{-17}$[43] (or $<1.1 \times 10^{-17}$)[44] s^{-1} molecule^{-1} cm^3. This value translates to $\Delta G^{\ddagger} = 12.1$ (12.2) kcal mol^{-1}. By inspecting Figure 1, it can be noted that the DFT estimate deviates from the experimental datum by 4.5 (NO_3) or 0 (HO) kcal mol^{-1}. The CBS-QB3 data deviate less than DFT in the former case, but more in the latter, namely by -1.8 or -1.1 kcal mol^{-1}. The U-CBS-QB3 data perform similarly, differing by 1.0 or 5.7 kcal mol^{-1}, respectively. Considering now the addition of NO_2, for which no experimental data are apparently available, it can be seen that the DFT result is closer to the U-CBS-QB3 (+0.9 kcal mol^{-1}) than to CBS-QB3 (+3.5 kcal mol^{-1}). The (standard) CBS-QB3[32] and the (recommended)[33b] U-CBS-QB3 data differ, in turn, by 2.6 (NO_2), 2.7 (NO_3), or even 6.8 (HO) kcal mol^{-1} between themselves. All these data suggest that the DFT(B3LYP) method, used throughout this paper, can provide results of reliability comparable to the two versions of the CBS-Q composite method.

The computed DFT data discussed throughout this paper are therefore affected by some uncertainty. We cannot unfortunately define true error bars. However, this section has attempted to address this point: DFT overestimates (with respect to the experiment) the initial addition barriers within the 0.0−4.5 kcal mol^{-1} range. However, we do not aim to estimate absolute rates, rather v ratios, for which some cancellation of the errors can be expected.

Naphthalene. The three radical attacks by NO_2, NO_3, and HO were studied in a parallel way also for the 1 and 2 positions of naphthalene (**N**). These attacks are shown in Scheme 3 for position 1 only, and labeled as reaction 1, 2, and 3, respectively. The energetics are collected in Table 2. The direct addition of NO_2, which yields the nitrocyclohexadienyl radical adducts **1-N-I** and **2-N-I** (reaction **1**), is somewhat less endothermic and endoergic than for benzene, more so for position 1. The free energy differences are larger than the enthalpy differences by 9−10 kcal mol^{-1} in all cases. Consistently, the relevant barriers are estimated to be substantial, but lower than that for benzene: $\Delta G^{\ddagger} \approx 25$ and 29 kcal mol^{-1}, respectively, vs 30 kcal mol^{-1} for the nitrocyclohexadienyl radical adduct **B-I** (position 1 is more reactive then 2, as expected for an electrophilic radical attack).

The attacks by the nitrate radical, which produce the nitroxybenzocyclohexadienyl radical intermediates **1-N-II** and **2-N-II** (reaction 2), though slightly exothermic (ΔH), are endoergic ($\Delta G = 7$ and 12 kcal mol^{-1}, respectively; compare the 13 kcal mol^{-1} value for the nitroxy intermediate **B-II**). The free energy barriers are likewise lower than those for benzene: $\Delta G^{\ddagger} \approx 12$ and 15 kcal mol^{-1}, respectively, to be compared with 17 kcal mol^{-1} for **B-II**. These data are in qualitative agreement with the rate constants measured by Atkinson et al.[44]

By contrast, the attack by hydroxyl, which produces the hydroxybenzocyclohexadienyl radical intermediates (**1-N-III** and **2-N-III**, reaction 3), is sharply exothermic, to such an extent

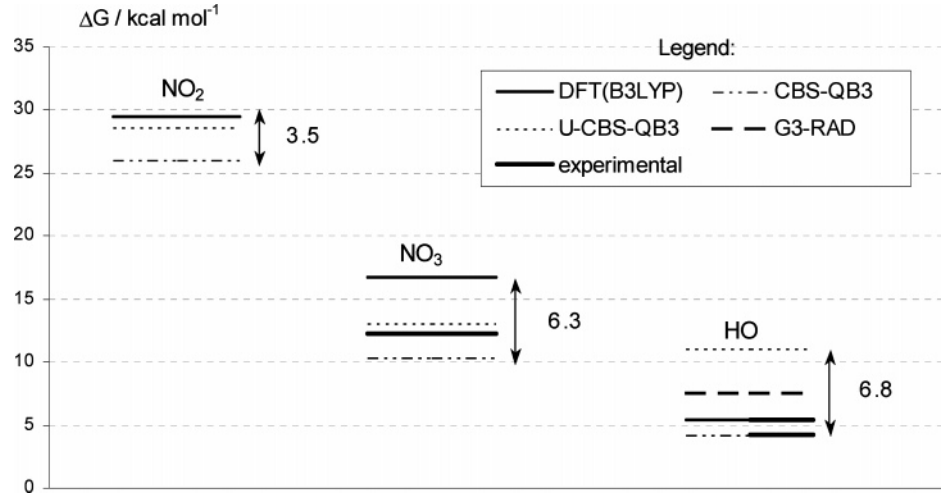

Figure 1. Free energy barriers for the addition of NO_2, NO_3, or HO to benzene (see Scheme 1), estimated by different methods. Experimental values: for HO, ref 42; for NO_3 (only an estimate available), ref 43.

SCHEME 3

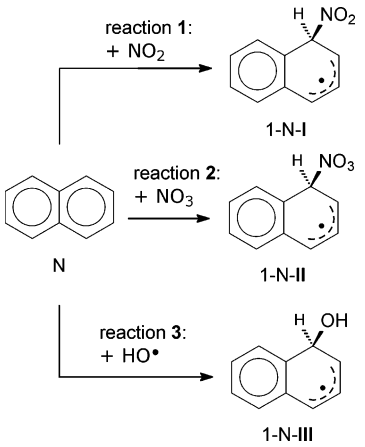

that negative free energy differences are still obtained: $\Delta G = -13$ and -8 kcal mol^{-1}, respectively (-7 kcal mol^{-1} for the analogous hydroxy intermediate **B-III**). The free energy barriers are estimated as $\Delta G^{\ddagger} \approx 4$ and 6 kcal mol^{-1}, respectively (5 kcal mol^{-1} for **B-III**). Therefore, the reverse reaction is easier for the nitroxy intermediate **N-II** than for the hydroxy **N-III**, in agreement with the experimental findings.[9,14]

The entropy term is unfavorable for all addition reactions, as expected, and raises the barrier by 9−13 kcal mol^{-1}, at room temperature, with respect to the enthalpy difference values.

The estimates of the *G* barrier height in correspondence of the TS geometry on the *E* surface is refined again by means of a couple of constrained optimizations at shorter and larger N−C or O−C distance. Since for position 1 this procedure confirms again in all three cases of Table 2 the geometrical location of the maximum along the *G* profile in correspondence of the TS (with a very small refinement of the barrier values), the constrained optimizations were not carried out for position 2.

Rate ratios can again be roughly estimated by setting the NO_2, NO_3, and HO concentrations as done above for benzene. Taking for instance position 1, $k_{NO_2}/k_{NO_3} \approx 2 \times 10^{-10}$ and $k_{NO_2}/k_{HO} \approx 6 \times 10^{-16}$, at $T = 298$ K. Then, $v_{NO_2}/v_{NO_3} \approx 10^{-6}$ again, and $v_{NO_2}/v_{HO} \approx 10^{-10}$. They are almost as adverse to direct nitration as for benzene (yet, the change from 10^{-12} to 10^{-10} in comparing NO_2 with HO could suggest some attenuation in proceding to larger systems: work is in progress on this point).

The *G* profiles have to be redefined at the higher temperature by performing the vibrational analysis as already described. The barrier height becomes 57 kcal mol^{-1} for NO_2 and the maximum occurs at $R = 1.79$ Å (1.89 Å at room temperature). For HO it is 32 kcal mol^{-1} ($R = 1.98$ Å, 2.18 Å at room temperature). Again, the NO_3 data in Table 1 are reported for the sake of completeness, though its concentration is expected be quite small under these conditions. The NO_2 attack is more difficult than that by HO by ca. 25 kcal mol^{-1}, which gives a situation similar to that found for benzene: $k_{NO_2}/k_{HO} \approx 3 \times 10^{-5}$ at $T = 1200$ K and, consequently, the rate ratio is presumably in favor of the HO attack (high HO concentrations can be found in correspondence of different combustion situations).[38] From Table 2 it can also be seen that the reverse process is easier for the nitrocyclohexadienyl radical adduct **N-I** than for the hydroxy analogue **N-III**.

Then, as done for benzene, the effectiveness of N_2O_5 as a gas-phase nitrating agent was further explored for position 1 of naphtalene (reaction 4). Only the attack that proved to be easier on benzene, illustrated in Scheme 2b, was explored for naphthalene, and produced $\Delta G^{\ddagger} = 36.1$ kcal mol^{-1} (Table 2). This negative result is similar to that of benzene, and rules out any role of N_2O_5 as a gas-phase nitrating agent. By contrast, the kinetic constant values measured by Pitts and co-workers[36] (2×10^{-17} to 3×10^{-17} molecule^{-1} cm^3 s^{-1}) would be consistent with a *G* barrier of ca. 13 kcal mol^{-1}. This quantity is, curiously enough, close to the barriers for the attack of NO_3, 11.8 and 15.1 kcal mol^{-1}, for the attacks in positions 1 and 2, respectively. However, an initial attack by this species was dismissed by those authors.[36] Due to the intrinsic capabilities and limitations of the theoretical methods employed (see Figure 1), we can in fact aim more to assess branching ratios, rather than to compute rate constant absolute values (this is a well-known issue).[47] Yet, a difference of 22−23 kcal mol^{-1}, much larger than the deviations of DFT from experiment discussed above, allows us to confidently maintain that nitrogen pentoxide cannot be an effective nitrating agent. However, we point out that in more recent studies Atkinson et al.[48] consider that "under conditions where N_2O_5, NO_3 radicals and NO_2 are in equilibrium, these reactions are kinetically equivalent to a reaction with N_2O_5". Our results support nitrate as the attacking species.

Further Transformations of the Intermediates. Notwithstanding the results of the preceding section, to assess the contribution given by each pathway to the production of the final nitroarene, the subsequent steps involving the intermediates **I**−**III** have to be explored.

SCHEME 4

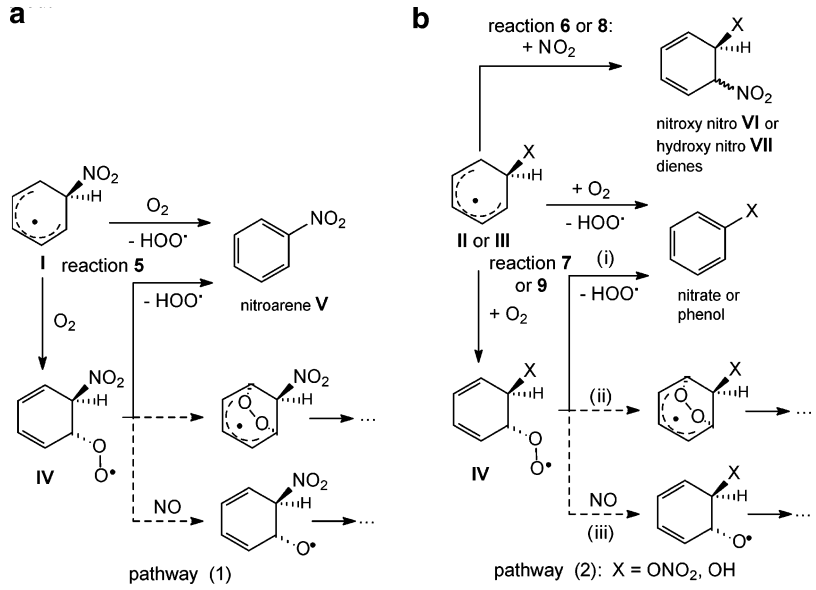

Pathway 1: *H Abstraction, which Follows Direct Nitration.* The direct nitration pathway opened by the attack of nitrogen dioxide (reaction 1) must, to give the nitroarene product **V**, to undergo the abstraction of the hydrogen *gem* to the nitro group in the three nitro intermediates **B-I**, **1-N-I**, and **2-N-I**. Dioxygen, considered as the most likely abstractor, can operate in two ways: (i) by direct one-step H abstractionor (ii) via addition to the π unsaturated radical system (*ortho* to the nitro-substituted carbon, to give peroxyl intermediates **IV**), followed by loss of hydroperoxyl radical (as exemplified for benzene under the collective label "reaction 5" in Scheme 4a). However, dioxygen addition can also open other pathways,[14−17] as shown again in Scheme 4a (dashed arrows).

Pathway 2: *NO_2 Addition, Followed by Nitric Acid or Water Elimination.* The **II** and **III** radical intermediates, generated by the addition of the nitrate (reaction 2) and hydroxyl (reaction 3) radicals, can easily add nitrogen dioxide (reactions 6 and 8) (though in competition with dioxygen, reaction 7, as shown in Scheme 4b) to produce closed shell nitroxy-nitro or hydroxy-nitro intermediates **VI** and **VII**, respectively. Though the evolution of these rather stable closed shell molecules **VI** and **VII** can obviously be diverse (e.g., further attacks by HO or NO_3, then by O_2, etc.), in this study only the nitric acid or water elimination step that produces the final nitroarenes is explored.

Pathways 1 and 2 just outlined now will be discussed in more detail for benzene and naphthalene.

Benzene. Pathway 1: The H abstraction by O_2 from the nitro adduct **B-I** can take place in one step, which requires 14 kcal mol^{-1} (reaction 5). As an alternative, the two-step pathway presents a first *G* barrier of 19 kcal mol^{-1} for O_2 addition, to give the peroxyl adduct **IV**, from which hydroperoxyl loss entails a second barrier of less than 4 kcal mol^{-1} (Table 3).

Pathway 2: Addition/elimination steps. Further NO_2 addition to the nitro- and hydroxycyclo-hexadienyl radical intermediates **B-II** or **B-III** can produce four adducts through reactions 6 or 8. These are the 1,2 and 1,4 nitroxy-nitro dienes **B-VI**, or the hydroxy-nitro analogues **B-VII** (both as *cis* or *trans* isomers: wavy bond in Scheme 4b). Of these, the *trans* 1,2 isomers can be envisaged as inclined to undergo a favorable HNO_3 or H_2O elimination step (Scheme 5).

In fact, the **B-VI** and **B-VII** isomers are closed shell molecules, and thus relatively stable. Accordingly, their further

SCHEME 5

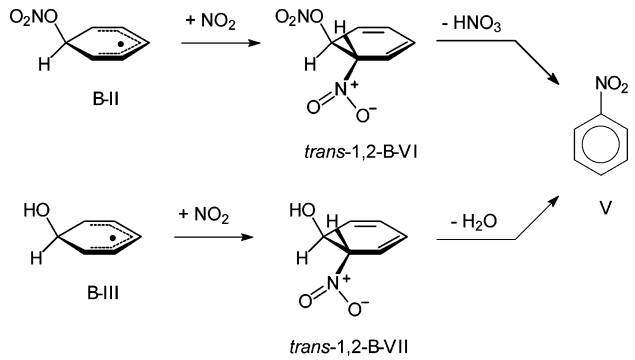

evolution should imply a bimolecular step, as the attack of some reactive radical species.[45] However, if we consider in particular those 1,2 isomers in which the vicinal nitroxy or hydroxy groups are *trans* to the nitro, a monomolecular step to yield nitrobenzene **V** is conceivable.

Further Reactions of the Nitroxycyclohexadienyl Radical Intermediate B-II. The *anti* addition of NO_2 to the radical **B-II** (Scheme 4b, reaction **6**), in the ortho position, yields the *trans*-1,2-**B-VI** adduct without any energy barrier, and is exoergic by 27 kcal mol^{-1}. Though a free energy gain of −10 kcal mol^{-1} is still estimated (Table 3), a free energy barrier could be present. Also O_2 could add to **B-II**, giving a peroxyl radical adduct **IV**, which is located 11.0 kcal mol^{-1} above the reactants. Moreover, O_2 could perform a H abstraction from the X-substituted carbon (Scheme 4b, reaction **7**). However, in the case of the nitroxy radical **B-II**, no transition structure for this process could be defined.

To assess the feasibility of the nitration step, the free energy barriers for the competing attacks to the nitroxy intermediate **B-II** by NO_2 or O_2 have been approximately assessed. For the attack of nitrogen dioxide the estimate is somewhat laborious, since no maximum along the energy profile is present, and a maximum can be found only along the approximate free energy profile itself. A series of constrained optimizations on the NO_2 + **B-II** system was carried out, in which the energy was minimized in correspondence of fixed values of the distance *R* between the incoming NO_2 nitrogen and the ortho carbon. For each point, *G* was estimated by projecting out the imaginary

frequency related to the relative motion along *R*. The *G* profile so obtained had a maximum for the rather large value $R = 4.0$ Å, and the best estimate of the barrier height is 8 kcal mol^{-1}. In the case of the competing attack by dioxygen, though a straightforward estimate of the free energy barrier height is possible, as a TS on the energy hypersurface is present (the computation of *G* in correspondence of the TS would give a barrier estimate of 18 kcal mol^{-1}), a couple of constrained optimizations yields a refined value of 19 kcal mol^{-1}, in correspondence of the ortho carbon−oxygen distance $R = 1.95$ Å (the profile is in this case somewhat more precisely defined).

Once the O_2 addition barrier is defined, a standard steady-state treatment could be carried out to estimate k_{O_2}, the overall rate constant for the "O_2 pathway". The treatment involves the O_2 addition to give the peroxyl intermediate **IV**, which has just been described, as well as its further evolution. Four main steps from **IV** can be considered: (i) HOO elimination to give the aromatic nitrate, (ii) ring closure to an endoperoxide intermediate, (iii) O abstraction by NO, and (iv) the backward step from **IV** to the nitroxycyclohexadienyl radical intermediate **B-II** plus O_2. Actually, step i requires only 3 kcal mol^{-1} starting from **IV**. By contrast, step ii is rather difficult, since it requires ca. 17 kcal mol^{-1}, and can be safely discarded. The easy step i corresponds to a rate constant that can be compared to the experimental *k* for the competitive process iii.[46] The rate ratio is of the order of 10^9, in favor of the former. Thus, also step iii can be discarded. On the other hand, the backward process iv requires 8 kcal mol^{-1}. In conclusion, the steady-state treatment is not necessary in this case, for the steps involving **IV** and its evolution, and k_{O_2} is numerically equivalent to the rate constant for the addition step producing **IV**. The treatment is not carried out also for nitrogen dioxide, as it adds irreversibly to give a closed shell intermediate (k_{NO_2}). Thus, on the basis of these estimates, the rate constant ratio $k_{NO_2}/k_{O_2} \approx 2 \times 10^8$ ($T = 298$ K). The kinetic constant ratio factor is counterbalanced by the fact that the O_2 concentration is overwhelmingly high with respect to any realistic NO_2 concentration. The rate ratios for the NO_2 and O_2 tropospheric channels can be approximately assessed by setting the O_2 concentration to ca. 10^{18} molecules cm^{-3}, and $[NO_2]$ to 10^8 or 10^{12}, relevant to unpolluted or polluted situations, respectively. In the two cases, the branching ratios are given by $v_{NO_2}/v_{O_2} \approx 1$, or 10^4, respectively, at 298 K. Therefore, the nitration pathway can even prevail, with formation of the **B-VI** intermediate.

Under combustion conditions, say at 1200 K, a similar assessment of the free energy profiles provides much higher barriers. The barrier height is 48 kcal mol^{-1} for NO_2 and the maximum occurs at $R = 2.4$ Å. For O_2 it is even higher (52 kcal mol^{-1}) and is found at $R = 2.05$ Å. The same considerations about the steady-state treatment apply, since process i is easy. Thus, during combustion, the attack by NO_2 is favored by almost 5 kcal mol^{-1}, which gives a rate constant ratio $k_{NO_2}/k_{O_2} \approx 7$. If $[NO_2]$ is set to even 10^{13} molecules cm^{-3}, which could be considered as a peak concentration in a combustion situation, the branching ratio becomes $v_{NO_2}/v_{O_2} \approx 10^{-4}$ ($T = 1200$ K).

The subsequent HNO_3 elimination step (the TS is displayed in Figure 2) could be slower of faster, depending on the thermalization of **B-VI**. In fact, with a free energy barrier of 17 kcal mol^{-1} with respect to the **B-VI** intermediate (35 kcal mol^{-1} at $T = 1200$ K), the TS is set by the exoergicity of the preceding step at 7 kcal mol^{-1} above the nitroxycyclohexadienyl adduct **B-II** (62 kcal mol^{-1} at $T = 1200$ K).

Further Reactions of the Hydroxycyclohexadienyl Radical Intermediate B-III. Similarly, the formation of *trans*-1,2-**B-VII** (Scheme 4b, reaction **8**, and Scheme 5) presents no energy barrier and is associated to a free energy gain of −11 kcal mol^{-1} (Table 3). The procedure based on constrained optimizations outlined above provides estimates for the *G* barriers for the addition onto the hydroxy intermediate **B-III** of 8 kcal mol^{-1} for NO_2, with *G* maximum at $R = 3.6$ Å, and of 18 kcal mol^{-1} for O_2, with *G* maximum at $R = 1.97$ Å (see reactions 8 and 9, in Scheme 4b). However, in this case, the direct H abstraction operated by O_2 onto the hydrogen geminal to the hydroxyl is favored over the addition by almost 5 kcal mol^{-1}. It it thus the phenol formation that competes with NO_2 addition.

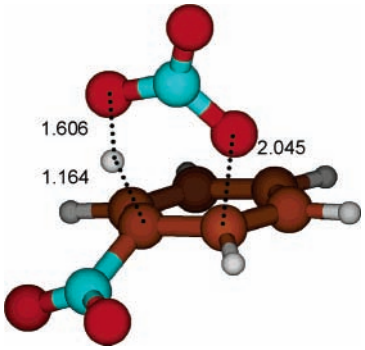

Figure 2. TS for HNO_3 elimination.

The attack by NO_2 is favored over that of O_2 by an estimated rate constant ratio $k_{NO_2}/k_{O_2} \approx 9 \times 10^3$. This approximate guess provides (same $[NO_2]$ and $[O_2]$ values as for the nitroxy intermediate **B-II**), at 298 K, branching ratios $v_{NO_2}/v_{O_2} \approx 10^{-6}$, or 10^{-2}, for an unpolluted or polluted situation, respectively.

At 1200 K, a similar assessment of the free energy profiles provides much higher barriers. The barrier height becomes 40 kcal mol^{-1} for NO_2 and the maximum occurs at $R = 2.4$ Å, as in the preceding case. For O_2 addition it is 52 kcal mol^{-1}, and corresponds to $R = 1.97$ Å. However, also at this temperature the direct H abstraction by O_2 onto the hydrogen geminal to the hydroxyl prevails, by ca. 10 kcal mol^{-1}. Thus, under combustion conditions, the attack by NO_2 is comparable with H abstraction (the barrier is lower by 2 kcal mol^{-1}), which gives a rate constant ratio $k_{NO_2}/k_{O_2} \approx 2$. If $[NO_2]$ is set again to the hypothesized peak concentration of 10^{13} molecules cm^{-3}, the branching ratio at 1200 K becomes $v_{NO_2}/v_{O_2} \approx 10^{-5}$.

The subsequent H_2O elimination step, however, requires overcoming a very high free energy barrier (38 kcal mol^{-1} with respect to the **B-VII** diene, 40 kcal mol^{-1} at $T = 1200$ K). As this cannot be compensated by the previous step (the TS is still almost 27 kcal mol^{-1} above the nitroxy intermediate **B-II** adduct, 67 kcal mol^{-1} at $T = 1200$ K), the H_2O elimination pathway does not seem promising. Comparing the H_2O and the HNO_3 eliminations, it can be noted that at 1200 K their energetics become more similar.

The steps considered in this section see a barrier 14 kcal mol^{-1} high for H abstraction, pathway 1, and 7−8 kcal mol^{-1} high for addition/elimination, pathway 2. Since the first step was much easier for the HO or NO_3 attacks than for NO_2, the overall picture confirms that pathway 1 is quite unlikely. However, also the initial easy attack carried out by hydroxyl is not sufficient to finally yield the nitroaromatic product, since the third and last step is demanding. This seems to suggest that only the pathway opened by the nitrate radical can be effective in producing nitrobenzene. To illustrate the evolution of benzene to nitrobenzene, the free energy profiles at $T = 298$ K are displayed in Figure 3a.

Finally, we have explored the possible 1,2 migration of the NO_2 or HO groups in the nitrocyclohexadienyl radical adduct

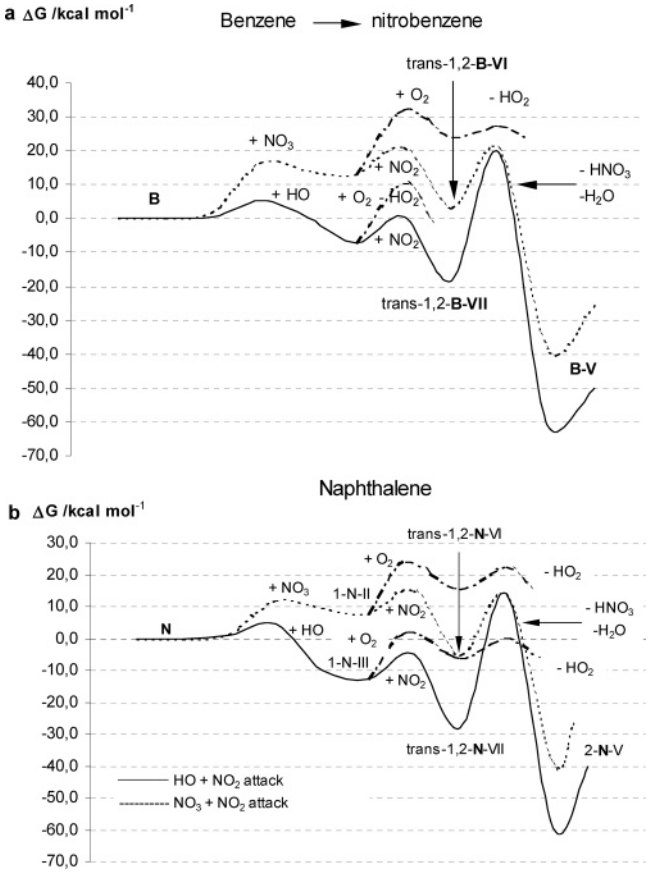

Figure 3. Free energy profiles (298 K) for the evolution of (a) benzene (**B**) to nitrobenzene (**B-V**) and (b) naphthalene (**N**) to 2-nitronaphthalene (2-**N**-**V**), via HO or NO_3 attack (for **N** in position 1), followed by trans NO_2 addition on the adjacent position, and final HX elimination (X = HO or NO_3). In competition with NO_2 addition, O_2 can abstract one H (see text). The two reactant levels have been made coincident.

SCHEME 6

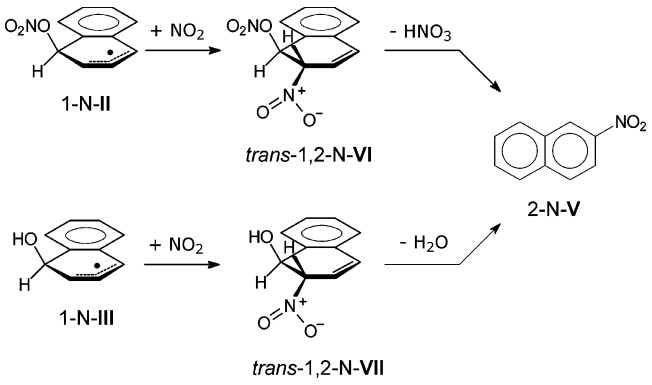

B-I and its hydroxy analogue **B-III**, respectively. No TS was found, since both OH and NO_2 prefer to dissociate. Then, the 1,2 migration of the hydrogen geminal to HO was also explored in the hydroxycyclohexadienyl radical. This migration takes place, but requires overcoming rather high barriers ($\Delta E^{\ddagger} = 33.6$, $\Delta H^{\ddagger} = 32.1$, $\Delta G^{\ddagger} = 40.5$ kcal mol^{-1}).

Naphthalene. We will first deal with the pathway that potentially leads to 2-nitronaphthalene. This is of the addition/elimination type (Pathway 2, Scheme 6). Since the addition of NO_2 to the nitroxy and hydroxy radical intermediates **N-II** and **N-III** is a radical coupling (the processes are the same as those labeled as "reaction 8" and "reaction 9" for benzene, see Scheme 4b), NO_2 adds preferentially to the positions having the higher spin density, i.e., to position 1 if it was carried out in 2 (or to positions 2 and 4 if the first NO_3 or HO attack was in 1). All the resulting nitroxy-nitro **VI** or hydroxy-nitro **VII** intermediates are closed shell molecules, thus rather stable. Of them, only the *trans* vicinal isomers can give way to a further elimination step of HNO_3 or H_2O, which yields the product (as illustrated for 2-nitronaphthalene in Scheme 6). The other isomers can be subject to further attacks by reactive species. To exemplify the evolution of a naphthalene system to its nitroaromatic analogue, the free energy profiles for the formation of 2-nitronaphthalene are displayed in Figure 3b. Following the initial attack of HO or NO_3 in position 1, trans NO_2 addition on the adjacent position and final HX elimination (X = HO or NO_3) lead to 2-nitronaphthalene.

Further Reactions of the Nitroxybenzocyclohexadienyl Radical Intermediate 1-N-II. The *anti* addition of NO_2 to position 2 of the radical **1-N-II** yields the *trans*-1,2-**N-VI** adduct without any energy barrier, and is exoergic by 13 kcal mol^{-1} in terms of *G*, at room temperature (Table 4). To approximately assess the free energy barriers for the competing attacks to **1-N-II** by NO_2 or O_2, two series of constrained optimizations on the reacting systems were carried out, as done for the case of benzene. The *G* profile obtained in the case of NO_2 presents a maximum for the rather large value $R = 3.7$ Å, and the estimate of the barrier height is 8 kcal mol^{-1}. In the case of the competing attack by dioxygen, the barrier height is 16 kcal mol^{-1}, in correspondence of $R = 1.99$ Å. Once the addition barriers are defined, the steady-state treatment is carried out to estimate k_{O_2}, the overall rate constant for the "O_2 pathway". The same steps considered for benzene, and originating from the peroxyl adduct, are taken into account: (i) the HOO elimination, (ii) the ring closure, (iii) O abstraction by NO (for which an experimental *k* is used again), and also (iv) the backward step to give again the nitroxy adduct plus O_2. The ring closure entails a high barrier and is not considered. Step i is compared to the experimental *k* for step iii.[46] The rate ratio (almost 10^7 even in a polluted situation) favors the HOO loss. Thus, also step iii can be discarded. The backward process iv requires 9 kcal mol^{-1}. In brief, the steady-state treatment gives $k_{addO_2} = 7.7 \times 10^{-21}$ s^{-1} molecule^{-1} cm^3 for the pathway related to O_2 addition. This is now added to the rate constant for H abstraction by O_2 ($k_{abs} = 1.6 \times 10^{-20}$ s^{-1} molecule^{-1} cm^3), and gives $k_{O_2} = 2.4 \times 10^{-20}$ s^{-1} molecule^{-1} cm^3. On the basis of these estimates, the rate constant ratio $k_{NO_2}/k_{O_2} \approx 1 \times 10^6$ ($T = 298$ K). This result is of the same order of magnitude of the experimental datum by Sasaki et al. ($k_{NO_2}/k_{O_2} \approx 2.5 \times 10^6$), measured for naphthalene.[14,15] Consequently, the branching ratios are $v_{NO_2}/v_{O_2} \approx 10^{-4}$, or 1, in unpolluted or polluted situations, respectively.

At 1200 K, the *G* profile obtained for the NO_2 attack presents a maximum for $R = 2.30$ Å, and the estimate of the barrier height is 41 kcal mol^{-1}. For the attack of O_2, the barrier is 50 kcal mol^{-1} and occurs at $R = 1.99$ Å. So, the attack by NO_2 is favored by 8 kcal mol^{-1}, and $k_{NO_2}/k_{O_2} \approx 3 \times 10^1$. If [$NO_2$] is set as before to 10^{13} molecules cm^{-3} (taken as the greatest concentration in a combustion situation) the branching ratio at 1200 K becomes $v_{NO_2}/v_{O_2} \approx 10^{-4}$.

The following HNO_3 elimination step has a *G* maximum 19 kcal mol^{-1} above the adduct, but only 6 kcal mol^{-1} above the nitroxybenzocyclohexadienyl radical intermediate **N-II** (relevant to the hypothesis that the adduct does not reach thermal equilibrium with the medium before HNO_3 loss takes place). At $T = 1200$ K, a similar *G* difference with respect to the adduct is found, 20 kcal mol^{-1}, which however, rise to 44 kcal mol^{-1},

if reference to **N-II** is made. Thus, the extent of thermalization of the adduct could play a role as regards the feasibility of this step.

Evolution of the Hydroxybenzocyclohexadienyl Radical Intermediate 1-N-III. The formation of *trans*-1,2-**N-VII** (Scheme 6) goes much the same way, with no energy barrier, and is associated to a free energy gain of 15 kcal mol^{-1} (Table 4). The estimates of the *G* barriers for the attacks onto the intermediate **1-N-III** are 8 kcal mol^{-1} for NO_2, with a *G* maximum at the large value of $R = 4.1$ Å, and of 15 kcal mol^{-1} for O_2, with the *G* maximum at $R = 1.94$ Å.

Once the O_2 addition barrier is defined, the steady state allows us to estimate k_{O_2}, the overall rate constant for the "O_2 pathway", to which the four steps (i−iv) defined above contribute. The two ring closures (step ii), to give 2,3 and 2,4 endoperoxides, present very high barriers and are discarded. The easy step i is compared to the experimental *k* for step iii,[46] and the rate ratio is on the order of 10^8, in favor of the former: thus, also (iii) can be discarded. On the other hand, the backward process iv requires 8 kcal mol^{-1}. In conclusion, the steady-state treatment gives $k_{addO_2} = 1.7 \times 10^{-19}$ s^{-1} $molecule^{-1}$ cm^3. This is to be added to the rate constant for H abstraction ($k_{abs} = 1.2 \times 10^{-19}$ s^{-1} $molecule^{-1}$ cm^3). This gives $k_{O_2} = 2.9 \times 10^{-19}$ s^{-1} $molecule^{-1}$ cm^3. Thus, on the basis of these estimates, the rate constant ratio $k_{NO_2}/k_{O_2} \approx 8 \times 10^4$ ($T = 298$ K). Consequently, the branching ratios are $v_{NO_2}/v_{O_2} \approx 10^{-5}$, or 10^{-1}, in the unpolluted and polluted situations, respectively. The formation of 2-nitronaphthalene is more advantageous by 1 order of magnitude when starting with NO_3 as attacking species with respect to HO. This result can be compared with the results of Sasaki et al. (Table 2 in ref 14), which report a factor of ca. 10 in favor of NO_3 as initial attacking species. In any case, here the subsequent water loss in **VII** is again demanding (Table 4). Therefore, the nitration pathway can only slightly contribute in the HO case.

At 1200 K, the *G* profile for the NO_2 attack has a maximum of 39 kcal mol^{-1} at $R = 2.30$ Å, while O_2 addition presents a maximum 47 kcal mol^{-1} high at $R = 1.94$ Å. At this temperature the HOO elimination from the peroxyl adduct becomes very easy. Therefore we can simply add the rate constants for O_2 addition and H abstraction, and obtain $k_{O_2} = 3.3 \times 10^{-16}$ s^{-1} $molecule^{-1}$ cm^3. Therefore $k_{NO_2}/k_{O_2} \approx 10$. With $[NO_2] = 10^{13}$ molecules cm^{-3}, the branching ratio becomes $v_{NO_2}/v_{O_2} \approx 10^{-4}$.

Let us now turn to the formation of 1-nitronaphthalene: both Pathway 1 and Pathway 2 are considered (Table 5). As concerns Pathway 1, the one-step H abstraction from the nitro adduct **1-N-I** (NO_2 in position 1), operated by O_2, requires 19 kcal mol^{-1} at $T = 298$ K (almost 50 kcal mol^{-1} at $T = 1200$ K). The two-step variant presents a first *G* barrier of 16 kcal mol^{-1} for O_2 addition (in position 2), to give the peroxyl adduct, and then, from the adduct, a second barrier of 9 kcal mol^{-1} for hydroperoxyl loss (49 and 10 kcal mol^{-1}, respectively, at $T = 1200$ K). Both alternatives would give 1-nitronaphthalene.

Pathway 2 has to do with the nitroxy and the hydroxy intermediates **2-N-II** and **2-N-III**.

Evolution of the Nitroxybenzocyclohexadienyl Radical Intermediate 2-N-II. The *anti* addition of NO_2 to position 1 of the radical **2-N-II** yields the *trans*-1,2-**N-VI** adduct without any energy barrier, and is exoergic by 16 kcal mol^{-1} in terms of *G*, at room temperature (Table 5). To approximately assess the free energy barriers for the competing attacks to **1-N-II** by NO_2 or O_2, two series of constrained optimizations on the reacting systems were carried out again. The *G* profile obtained in the case of NO_2 presents a maximum for the rather large value $R = 3.80$ Å, and the estimate of the barrier height is ca. 8 kcal mol^{-1}. In the case of the competing attack by dioxygen, the barrier height is 10 kcal mol^{-1}, in correspondence of $R = 2.09$ Å.

Once the O_2 addition barrier is defined, the steady-state treatment is carried out to estimate k_{O_2}, the overall rate constant for the "O_2 pathway". This time, the direct H abstraction by O_2 is unlikely to contribute, because any attempt to define the relevant TS yields instead the HOO elimination TS from the peroxyl adduct (step i). Process i requires ca. 9 kcal mol^{-1}. The ring closure to give the 1,3 endoperoxide (step ii) presents, again, a very high barrier and is discarded. Also O abstraction by NO (step iii) can be discarded, as the rate ratio between steps i and iii is more than 10^5 even in a polluted situation. The steady-state treatement gives $k_{O_2} = 4.6 \times 10^{-17}$ s^{-1} $molecule^{-1}$ cm^3. The resulting rate constant ratio, $k_{NO_2}/k_{O_2} \approx 7 \times 10^2$ (at $T = 298$ K) gives finally the branching ratio $v_{NO_2}/v_{O_2} \approx 10^{-7}$, or 10^{-3}, for the unpolluted or polluted situations, respectively.

At 1200 K, the *G* profile obtained for the NO_2 attack presents a maximum for $R = 2.40$ Å, and the estimate of the barrier height is 37 kcal mol^{-1}. For the attack of O_2, the barrier is 42 kcal mol^{-1} high and occurs at $R = 1.99$ Å. At this temperature the steady-state treatment gives $k_{NO_2}/k_{O_2} \approx 2 \times 10^1$. With $[NO_2] = 10^{13}$ molecules cm^{-3}, the branching ratio becomes $v_{NO_2}/v_{O_2} \approx 10^{-4}$.

The final HNO_3 elimination step that follows has a *G* maximum 19 kcal mol^{-1} above that of the adduct **VI** (20 at $T = 1200$ K). However, at room temperature, if reference was made to the nitroxybenzo-cyclohexadienyl radical intermediate **2-N-II** (as if the adduct could not reach thermal equilibrium with the medium), the elimination would require only 3.4 kcal mol^{-1}. By contrast, the barrier rises in this case to 40 kcal mol^{-1} at $T = 1200$ K. Thus, the extent of thermalization of the adduct could play a role as regards the feasibility of this step.

Evolution of the Hydroxybenzocyclohexadienyl Radical Intermediate 2-N-III. The formation of *trans*-1,2-**N-VII** goes much the same way, with no energy barrier, and is associated to a free energy gain of 19 kcal mol^{-1}. Since the subsequent water loss is again very demanding, entailing a barrier 46 kcal mol^{-1} high, both at room temperature and 1200 K, it was evidently not promising to perform the complete set of optimizations carried out in the preceding cases.

Pyrene. We have also carried out a more limited set of calculations on the pyrene molecule. Taking for granted that the adducts with nitrate (**1-P-II**) and hydroxyl (**1-P-III**) can form rather easily (compare Figure 3), we have just assessed their energies and free energies relative to the separate reactants (see the Supporting Information). Then, the competition between nitrogen dioxide and dioxygen in adding to these radical intermediates, which is the key step to assess the extent of nitration, has been investigated by the same approach discussed above. The results are shown in Table 6. In terms of ΔG, and starting from **1-P-II**, NO_2 attack is easier than O_2 attack by 12.6 kcal mol^{-1}, at $T = 298$ K. At $T = 1200$ K, this difference reduces to 10.7 kcal mol^{-1}. A similar result is obtaind for **1-P-III**: NO_2 attack is again easier than O_2 attack by 13.2 kcal mol^{-1}, at $T = 298$ K, which reduces to 10.5 kcal mol^{-1} at $T = 1200$ K. The corresponding kinetic constant ratios are the following, at $T = 298$ K: $k_{NO_2}/k_{O_2} \approx 2 \times 10^9$ (for **1-P-II**) and $k_{NO_2}/k_{O_2} \approx 5 \times 10^9$ (for **1-P-III**). By setting again the O_2 concentration to ca. 10^{18} molecules cm^{-3}, and $[NO_2]$ to 10^8 or 10^{12}, relevant to unpolluted or polluted situations, respectively, we find $v_{NO_2}/v_{O_2} \approx 2 \times 10^{-1}$ or 2×10^3 for **1-P-II**, and $v_{NO_2}/v_{O_2} \approx 5 \times 10^{-1}$ or 5×10^3 for **1-P-III**. At $T = 1200$ K, $k_{NO_2}/$

TABLE 6: Pyrene: Steps from the 1-X-cyclohexadienyl-like Radical (X = Nitroxy, Hydroxy) to the *trans*-1-Nitronaphthalene

		$\Delta E^{a,b}$	ΔH^b $T = 298$ K	ΔG^b $T = 298$ K	ΔG^b $T = 1200$ K
1-nitroxypyrenyl radical + NO_2	**1-P-II** + NO_2	0.0	0.0	0.0	0.0
NO_2 addition "TS"[c,d]				9.8[d]	45.5[d]
trans-1-nitroxy-2-nitro adduct		−20.4			
O_2 addition TS[e]		*10.3*	*11.0*	*22.4*	56.2
trans-1-nitroxy-2-peroxyl adduct		*4.2*			
1-hydroxypyrenyl radical + NO_2	**1-P-III** + NO_2	0.0	0.0	0.0	0.0
NO_2 addition "TS"[c,f]				9.2[f]	43.4[f]
trans-1-hydroxy-2-nitro adduct		−21.4			
O_2 addition TS[e]		*11.1*	*11.7*	*22.5*	*53.9*
trans-1-hydroxy-2-peroxyl adduct					

[a] From corrected DFT(B3LYP)/6-311+(2df,p)//6-31G(d) energy values. [b] Units: kcal mol^{-1}. [c] Maximum along a G profile generated in correspondence of an all-downhill E profile. [d] In correspondence of a distance r(N−C) = 2.30 Å, at $T = 298$ K, and 2.20 Å, at $T = 1200$ K. [e] The maxima for O_2 addition are determined as described in the main text, and are referred to as **P-II** or **P-III** + O_2 energy or free energy zero (in the case of dioxygen a TS on the energy surface is present). [f] In correspondence of a distance r(N−C) = 2.25 Å, at $T = 298$ K, and 2.20 Å, at $T = 1200$ K.

TABLE 7: Branching Ratios (v_{NO_2}/v_{O_2}) for the Attacks by NO_2 and O_2 on the Radical Intermediates Produced by Nitrate Attack (n-X-II) or Hydroxyl Attack (n-X-III)

	$T = 298$ K		$T = 12000$ K		$T = 298$ K		$T = 12000$ K
	$[NO_2]^a = 10^8$	$[NO_2]^a = 10^{12}$	$[NO_2]^a = 10^{14}$		$[NO_2]^a = 10^8$	$[NO_2]^a = 10^{12}$	$[NO_2]^a = 10^{14}$
from **B-II**:	1	10^4	10^{-3}	from **B-III**:	10^{-6}	10^{-2}	10^{-4}
from **1-N-II**:	10^{-4}	1	10^{-3}	from **1-N-III**:	10^{-5}	10^{-1}	10^{-3}
from **2-N-II**:	10^{-7}	10^{-3}	10^{-3}	from **2-N-III**:	not done	not done	not done
from **1-P-II**:	10^{-1}	10^3	10^{-2}	from **1-P-III**:	10^{-1}−1	10^3−10^4	10^{-2}

[a] Assumed concentrations in molecules cm^{-3}.

k_{O_2} drops to 9 or 8×10^1 (for **1-P-II** or **1-P-III**, respectively). By setting $[NO_2]$ to 10^{13}, the branching ratio becomes $v_{NO_2}/v_{O_2} \approx 9$ or 8×10^{-4} for **1-P-II** or **1-P-III**.

Table 7 provides a summary of the branching ratios estimated for the competition between nitrogen dioxide and dioxygen in adding to the initial radical intermediates, generated by NO_3 or HO attacks.

Conclusions

N_2O_5, NO_2, NO_3, and HO have been considered in this paper as possible reactive species to obtain nitrobenzene and the nitronaphthalenes as end products. N_2O_5 is ruled out as a possible nitrating agent, since its attack on the aromatic rings presents very high free energy barriers ($\Delta G^{\ddagger} \approx 36$ kcal mol^{-1}). The possible competition of the pathways set off by the other three molecules has been examined under tropospheric (1) and combustion (2) conditions.

(1) Tropospheric Conditions. The direct attack of the NO_2 radical on the aromatic is significantly more sluggish than that carried out by NO_3, and corresponds to a rate ratio of $v_{NO_2}/v_{NO_3} \approx 10^{-6}$ for both systems, and more so when compared to HO: $v_{NO_2}/v_{HO} \approx 10^{-12}$ (for benzene) and 10^{-10} (for naphthalene). If this attenuation had to proceed with increasing size of the aromatic system it would be interesting, and is presently under study.

Both the diurnal attack by HO and the analogous nocturnal addition of NO_3 open the way not only to nitration (outcome a) but also to several oxidative degradation pathways (outcome b), since further dioxygen addition to the nitroxy or hydroxy intermediates gives way to ring openings. This has to be considered when estimating the possible participation of nitrogen dioxide (as the first attacking radical) in the formation of the nitro-derivatives. To assess this point, the competing attacks of nitrogen dioxide (v_{NO_2}, outcome a) and dioxygen v_{O_2} (outcome b) on the first nitroxy or hydroxy intermediates have been studied at room temperature. On the nitroxy derivative of benzene, $v_{NO_2}/v_{O_2} \approx 1$−$10^4$ (to be read as corresponding to "unpolluted−polluted" situations), while on the hydroxy derivative $v_{NO_2}/v_{O_2} \approx 10^{-6}$−$10^{-2}$. On the 1-nitroxy derivative of naphthalene, $v_{NO_2}/v_{O_2} \approx 10^{-4}$−1, and on the 1-hydroxy derivative $v_{NO_2}/v_{O_2} \approx 10^{-5}$−$10^{-1}$. This set of data flanks those relevant to the first attack on the aromatic system, and indicates that the major contribution to nitroarenes comes from the HO and NO_3 initiated pathways. To illustrate this point, for each branching ratio, the datum on the right of the dash (polluted situation) has to be compared with those for direct nitration given above. For instance, taking the "polluted situation" hypothesis for benzene, if only one molecule undergoes a direct nitration by NO_2, with respect to 10^6 molecules attacked by nitrate, then for the pathway opened by nitrate, in correspondence of each intermediate attacked by dioxygen, 10^4 intermediates proceed by NO_2 addition.

(2) Combustion Conditions. By setting $T = 1200$ K, and hypothesizing a high NO_2 concentration (10^{13} molecules cm^{-3}), but a HO concentration 1 order of magnitude higher, the rate ratios are $v_{NO_2}/v_{HO} \approx 10^{-6}$ for both aromatics. Thus, rising temperature could put direct nitration on a slightly better ground. As regards the hydroxy derivatives of benzene and naphthalene, $v_{NO_2}/v_{O_2} \approx 10^{-5}$ and 10^{-4}, respectively (ca. 10^{-3} for pyrene). The major pathway for these intermediates will go through a peroxyl radical. The direct nitration pathway remains a very minor channel for nitration also at this temperature, though the difficult water elimination required as the last step of the pathway opened by hydroxyl could give it more importance.

A final comment on the tropospheric formation of the nitroarenes: the last step (elimination of nitric acid or water) can be more or less feasible, depending on the thermalization of the closed shell adduct that forms upon NO_2 addition onto the nitroxy- or hydroxy-aryl radical. If the adduct undergoes the elimination step before achieving thermal equilibrium, the barrier for HNO_3 elimination is rather low, 6−7 kcal mol^{-1}, but becomes 17−19 kcal mol^{-1} if the reverse is true. By

contrast, water elimination is very demanding in any case (from 27 to 38−42 kcal mol^{-1}).

Acknowledgment. We thank Dr. Ajith Perera for his assistance in the ACES II installation and optimal usage. Partial financial support by the Italian CNR (Agenzia 2000) and MIUR [PRIN-COFIN 2004, "Studio integrato sul territorio nazionale per la caratterizzazione ed il controllo di inquinanti atmosferici (SITECOS)"] is also acknowledged. This work was conducted in the frame of EC FP6 NoE ACCENT (Atmospheric Composition Change, the European NeTwork of Excellence).

Supporting Information Available: A listing of geometries, total energies, enthalpies, and free energies. This material is available free of charge via the Internet at http://pubs.acs.org.

References and Notes

(1) Becker, K. H.; Barnes, I.; Ruppert, L.; Wiesen P. Free radicals in the atmosphere: the motor of tropospheric oxidation processes. In *Free Radicals in Biology and Environment*; Minisci, F., Ed.; Kluwer Academic Publishers: Dordrecht, The Netherlands, 1997; Chapter 27, pp 365−385, and references therein.

(2) Güsten, H. Degradation of atmospheric pollutants by tropospheric free radical reactions. In *Free Radicals in Biology and Environment*; Minisci, F., Ed.; Kluwer Academic Publishers: Dordrecht, The Netherlands, 1997; Chapter 28, pp 387−408.

(3) Grosjean, D. *Sci. Total Environ.* **1991**, *100*, 367−414.

(4) Atkinson, R. Reactions of Oxygen Species in the atmosphere. In *Active Oxygen in Chemistry*; Valentine, J. S., Foote, C. S., Greenberg, A., Liebman, J. F., Eds.; Blackie Academic and Professional (Chapmann & Hall): London, UK, 1995; Chapter 7.

(5) Wayne, R. P. *Chemistry of Atmospheres*; Clarendon Press: Oxford, UK, 1996; pp 252−263.

(6) Finlayson-Pitts, B. J.; Pitts, J. N., Jr *Chemistry of the Upper and Lower Atmosphere*; Academic Press: London, UK, 2000; Chapter 10, sections E and F.

(7) (a) Homann, K.-H. *Angew. Chem., Int. Ed.* **1998**, *37*, 2434−2451. (b) A crystalline structure is defined as *turbostratic* when the basal planes are moved sideways relative to each other, bringing about a larger interplane distance with respect to a regular structure. If we compare soot to graphite, this irregular arrangement can come from the imperfect epitaxial growth of the soot particles, due in turn to a variety of defects. Thus, soot particles show superimposed (defective) graphenic layers which can be curved, and can be seen only locally as approximately parallel. The structure shown by soot globules can be more loosely said to be "onion-like" to describe the arrangement of the graphenic layers.

(8) See for instance: Reisinger, R. *Atmos. Environ.* **2000**, *34*, 3865−3874. Kirchner, U.; Scheer, V.; Vogt, R. *J. Phys. Chem. A* **2000**, *104*, 8908−8915. Pöschl, U.; Letzel, T.; Schauer, C.; Niessner, R. *J. Phys. Chem. A* **2001**, *105*, 4029−4041. Amman, M.; Kalberer, M.; Jost, D. T.; Tobler, L.; Rössler, E.; Piguet, D.; Gäggeler, H. W.; Baltensperger, U. *Nature* **1998**, *395*, 157−160. Arens, F.; Gutzwiller, L.; Baltensperger, U.; Gäggeler, H. W.; Amman, M. *Environ. Sci. Technol.* **2001**, *35*, 2191−2199. Lu're, B. A.; Mikhno, A. V. *Kinet. Catal.* **1997**, *38*, 490−497. Kamm, S.; Möhler, O.; Naumann, K.-H.; Saathoff, H.; Schurath, U. *Atmos. Environ*. **1999**, *33*, 4651−4661. Raisen, F.; Arey, J. *Environ. Sci. Technol.* **2005**, *39*, 64−73. Atkinson, R.; Arey, J. *Environ. Health Perspect.* **1994**, *102* (Suppl. 4), 117−126.

(9) (a) Atkinson, R.; Lloyd, A. *J. Phys. Chem. Ref. Data* **1984**, *13*, 315. (b) Atkinson, R. *J. Phys. Chem. Ref. Data* **1991**, *20*, 459−507.

(10) Atkinson, R.; Aschmann, S. M. *Int. J. Chem. Kinet.* **1994**, *26*, 929.

(11) Bolzacchini, E.; Bruschi, M.; Hjorth, J.; Meinardi, S.; Orlandi, M.; Rindone, B.; Rosenbohm E. *Environ. Sci. Technol*. **2001**, *35*, 1791−1797. Bolzacchini, E.; Meinardi, S.; Orlandi, M.; Rindone, B.; Hjorth, J.; Restelli, G. B. *Environ. Sci. Technol*. **1999**, *33*, 461−468.

(12) Feilberg, A.; Kamens, R. M.; Strommen, M. R.; Nielsen, T. *Atmos. Environ.* **1999**, *33*, 1231−1243.

(13) Amman, M.; Arens, F.; Gutzwiller, L.; Rössler, E.; Gäggeler, H. W. *EC/Eurotrac-2 Joint Workshop Proceedings, Aachen* **1999**, 236−239.

(14) Sasaki, J.; Aschmann, S. M.; Kwok, E. S.; Atkinson, R.; Arey, J. *Environ. Sci. Technol.* **1997**, *31*, 3173−3179.

(15) Atkinson, R.; Tuazon, E. C.; Bridier, I.; Arey, J. *Int. J. Chem. Kinet.* **1994**, *26*, 605−614.

(16) Ghigo, G.; Tonachini, G. *J. Am. Chem. Soc.* **1998**, *120*, 6753−6757.

(17) Ghigo, G.; Tonachini, G. *J. Am. Chem. Soc.* **1999**, *121*, 8366−8372.

(18) Motta, F.; Tonachini, G. *Atmospheric Diagnostics in Urban Regions*; Initiativen zum UmweltschutzsInitiatives for Environmental Protection Series; Erich Schmidt-Verlag: Berlin, Germany, 2001; Vol. 33, pp 120−128.

(19) Motta, F.; Ghigo, G.; Tonachini, G. *J. Phys. Chem. A* **2002**, *106*, 4411−4422.

(20) (a) Chung, G.; Kwon, O.; Kwon, Y. *J. Phys. Chem. A* **1997**, *101*, 4628−4632. (b) Vauthier, E.; Odiot, S.; Blain, M.; Fliszar, S. *THEOCHEM* **1998**, *423*, 195−201. (c) Bolzacchini, E.; Bruschi, M.; Galliani, G.; Hjorth, J.; Orlandi, M.; Rindone, B. *J. Phys. Org. Chem.* **2006**, *19*, 1−9.

(21) Ghigo, G.; Maranzana, A.; Tonachini, G.; Zicovich-Wilson, C. M.; Causà, M. *J. Phys. Chem. B* **2004**, *108*, 3215−3223.

(22) Maranzana, A.; Serra, G.; Giordana, A.; Tonachini, G.; Barco, G.; Causà, M. *J. Phys. Chem. A* **2005**, *109*, 10929−10939.

(23) Pople, J. A.; Gill, P. M. W.; Johnson, B. G. *Chem. Phys. Lett.* **1992**, *199*, 557−560. Schlegel, H. B. In *Computational Theoretical Organic Chemistry*; Csizsmadia, I. G., Daudel, R., Eds.; Reidel Publ. Co.: Dordrecht, The Netherlands, 1981; pp 129−159. Schlegel, H. B. *J. Chem. Phys.* **1982**, *77*, 3676−3681. Schlegel, H. B.; Binkley, J. S.; Pople, J. A. *J. Chem. Phys.* **1984**, *80*, 1976−1981. Schlegel, H. B. *J. Comput. Chem*. **1982**, *3*, 214−218.

(24) Parr, R. G.; Yang, W. *Density Functional Theory of Atoms and Molecules*; Oxford University Press: New York, 1989; Chapter 3. Becke, A. D. *Phys. Rev. A* **1988**, *38*, 3098−3100. Becke, A. D. *ACS Symp. Ser.* **1989**, *394*, 165. Pople, J. A.; Gill, P. M. W.; Johnson, B. G. *Chem. Phys. Lett.* **1992**, *199*, 557−560. Becke, A. D. *J. Chem. Phys.* **1993**, *98*, 5648−5652. Lee, C.; Yang, W.; Parr, R. G. *Phys. Rev. B* **1988**, *37*, 785−789.

(25) This theory level was tested on a model reaction, and compared with more expensive ab initio methods (Ghigo, G.; Tonachini, G. *J. Chem. Phys.* **1999**, *109*, 7298−7304), where it appeared to be a rather good compromise between reliability and feasibility in studying the degradation of aromatics.

(26) Hehre, W. J.; Ditchfield, R.; Pople, J. A. *J. Chem. Phys.* **1972**, *56*, 2257−2261. Hariharan, P. C.; Pople, J. A. *Theor. Chim. Acta* **1973**, *28*, 213−222. Clark, T.; Chandrasekhar, J.; Schleyer, P. v. R. *J. Comput. Chem.* **1983**, *4*, 294−301. Frisch, M. J.; Pople, J. A.; Binkley, J. S. *J. Chem. Phys.* **1984**, *80*, 3265−3269.

(27) Yamanaka, S.; Kawakami, T.; Nagao K.; Yamaguchi, K. *Chem. Phys. Lett.* **1994**, *231*, 25−33. Yamaguchi, K.; Jensen, F.; Dorigo, A.; Houk, K. N. *Chem. Phys. Lett.* **1988**, *149*, 537−542. See also: Baker, J.; Scheiner, A.; Andzelm, J. *Chem. Phys. Lett.* **1993**, *216*, 380−388. For discussions concerning the effect of spin projection on the performances of DFT methods, see: Wittbrodt, J. M; Schlegel, H. B. *J. Chem. Phys.* **1996**, *105*, 6574−6577. Goldstein, E.; Beno, B.; Houk, K. N. *J. Am. Chem. Soc.* **1996**, *118*, 6036−6043.

(28) Reaction enthalpies and free energies were computed as outlined, for instance, in: Foresman, J. B.; Frisch, Æ. *Exploring Chemistry with Electronic Structure Methods*; Gaussian, Inc.: Pittsburgh, PA, 1996; pp 166−168. McQuarrie, D. A. *Statistical Thermodynamics*; Harper and Row: New York, 1973; Chapter 8.

(29) Gonzalez, C.; Schlegel, H. B. *J. Chem. Phys.* **1989**, *90*, 2154−2161. Gonzalez, C.; Schlegel, H. B. *J. Phys. Chem.* **1990**, *94*, 5523−5527 and references therein.

(30) Gonzalez-Lafont, A.; Truong, T. N.; Truhlar, D. G. *J. Chem. Phys.* **1991**, *95*, 8875−8894. Hu, W.-P.; Liu, Y.-P.; Truhlar, D. G. *J. Chem. Soc., Faraday Trans.* **1994**, *90*, 1715−1725. Baboul, A. G.; Schlegel, H. B. *J. Chem. Phys.* **1997**, *107*, 9413−9417.

(31) Frisch, M. J.; Trucks, G. W.; Schlegel, H. B.; Scuseria, G. E.; Robb, M. A.; Cheeseman, J. R.; Montgomery, J. A., Jr.; Vreven, T.; Kudin, K. N.; Burant, J. C.; Millam, J. M.; Iyengar, S. S.; Tomasi, J.; Barone, V.; Mennucci, B.; Cossi, M.; Scalmani, G.; Rega, N.; Petersson, G. A.; Nakatsuji, H.; Hada, M.; Ehara, M.; Toyota, K.; Fukuda, R.; Hasegawa, J.; Ishida, M.; Nakajima, T.; Honda, Y.; Kitao, O.; Nakai, H.; Klene, M.; Li, X.; Knox, J. E.; Hratchian, H. P.; Cross, J. B.; Adamo, C.; Jaramillo, J.; Gomperts, R.; Stratmann, R. E.; Yazyev, O.; Austin, A. J.; Cammi, R.; Pomelli, C.; Ochterski, J. W.; Ayala, P. Y.; Morokuma, K.; Voth, G. A.; Salvador, P.; Dannenberg, J. J.; Zakrzewski, V. G.; Dapprich, S.; Daniels, A. D.; Strain, M. C.; Farkas, O.; Malick, D. K.; Rabuck, A. D.; Raghavachari, K.; Foresman, J. B.; Ortiz, J. V.; Cui, Q.; Baboul, A. G.; Clifford, S.; Cioslowski, J.; Stefanov, B. B.; Liu, G.; Liashenko, A.; Piskorz, P.; Komaromi, I.; Martin, R. L.; Fox, D. J.; Keith, T.; Al-Laham, M. A.; Peng, C. Y.; Nanayakkara, A.; Challacombe, M.; Gill, P. M. W.; Johnson, B.; Chen, W.; Wong, M. W.; Gonzalez, C.; Pople, J. A. *Gaussian 03*; Gaussian, Inc.: Pittsburgh, PA, 2003.

(32) CBS-Q//B3: Montgomery, J. A., Jr.; Frisch, M. J.; Ochterski, J. W.; Petersson, G. A. *J. Chem. Phys.* **2000**, *112*, 6532−6542. Montgomery, J. A., Jr.; Frisch, M. J.; Ochterski, J. W.; Petersson, G. A. *J. Chem. Phys.* **1999**, *110*, 2822−2827.

(33) G3-RAD: (a) Gómez-Balderas, R.; Coote, M. L.; Henry, D. J.; Radom, L. *J. Phys. Chem. A* **2004**, *108*, 2874−2883. (b) Henry, D. J.; Sullivan, M. B.; Radom, L. *J. Chem. Phys.* **2003**, *118*, 4849−4860.

(34) ACES II: Stanton, J. F.; Gauss, J.; Perera, S. A.; Watts, J. D.; Yau, A. D.; Nooijen, M.; Oliphant, N.; Szalay, P. G.; Lauderdale, W. J.;

Gwaltney, S. R.; Beck, S.; Balkov'a, A.; Bernholdt, D. E.; Baeck, K. K.; Rozyczko, P.; Sekino, H.; Huber, C.; Pittner, J.; Cencek, W.; Taylor, D.; Bartlett, R. J.—Integral packages included are VMOL (Almlöf, J.; Taylor, P. R.); VPROPS (Taylor, P. R.); ABACUS (Helgaker, T.; Jensen, H. J. Aa.; Jørgensen, P.; Olsen, J.; Taylor, P. R.); HONDO/GAMESS (Schmidt, M. W.; Baldridge, K. K.; Boatz, J. A.; Elbert, S. T.; Gordon, M. S.; Jensen, J. J.; Koseki, S.; Matsunaga, N.; Nguyen, K. A.; Su, S.; Windus, T. L.; Dupuis, M.; Montgomery, J. A.).

(35) (a) Atkinson, R.; Arey, J. *Atmos. Environ.* **2003**, *37* (Suppl. *2*), S197−S219. (b) Under combustion conditions, [NO] prevails over [NO_2] by approximately one order of magnitude (an estimate of the peak combustion concentration of both can be found in: http://www.afrinc.com/applications/combustion_monitoring/default.htm). (c) See for instance: Cheskis, S.; Derzy, I.; Lozovsky, V. A.; Kachanov, A.; Romanini, D. *Appl. Phys. B* **1998**, *66*, 377−381. Lozovsky, V. A.; Derzy, I.; Cheskis, S. *Twenty-Seventh Symposium* (*International*) *on Combustion*; The Combustion Institute, 1998; pp 445−452. Prisecaru, T.; Mihaescu, L.; Adam, A.; Bosoaga, A.; Prundianu, S.; Oprea, I.; Negreanu, G. Complex gas burner for an aeroderivative turbine; International Conference on Gas Turbine Technologies, Brussels, July 2003.

(36) Pitts, J. N., Jr.; Atkinson, R.; Sweetman J. A.; Zielinska, B. *Atmos. Environ.* **1985**, *19*, 701−705.

(37) Atkinson, R.; Arey, J.; Zielinska, B.; Aschmann, S. M. *Environ. Sci. Technol.* **1987**, *21*, 1014−1022

(38) Pitts, J. N., Jr.; Zielinska, B.; Sweetman J. A.; Atkinson, R.; Winer, A. M. *Atmos. Environ.* **1985**, *19*, 911−915.

(39) Pitts, J. N., Jr.; Sweetman J. A.; Zielinska, B.; Atkinson, R.; Winer, A. M.; Harger, W. P. *Environ. Sci. Technol.* **1985**, *19*, 1115−1121.

(40) Kamens, R. M.; Guo, J.; Guo, Z.; McDow, S. R. *Atmos. Environ.* **1990**, *24A*, 1161−1173.

(41) (a) In addition to these results, the data for the attack of the CH_3 radical to ethene, reported in ref 33b, can be compared. Inspection of Table 7 of ref 33b (entries CBS-QB3, U-CBS-QB3, and Experiment Gas Phase) for ethene (2nd column) suggests that the normal (spin-corrected) CBS-QB3 method gives the best match with the experimental value, being at variance at most by +0.5 to −1.7 kcal mol^{-1} (vs. +6.6 to +4.4 kcal mol^{-1} for U-CBS-QB3). (b) DeMatteo, M. P.; Poole, J. S.; Shi, X.; Sachdeva, R.; Hatcher, P. G.; Hadad, C. M.; Platz, M. S. *J. Am. Chem. Soc.* **2005**, *127*, 7094−7109. Barckholtz, C.; Barckholtz, T. A.; Hadad, C. M. *J. Phys. Chem. A* **2001**, *105*, 140−152. (c) Bartolotti, L. J.; Edney, O. E. *Chem. Phys. Lett.* **1995**, *245*, 119−122. Andino, J. M.; Smith, J. N.; Flagan, R. C.; Goddard, W. A., III; Seinfeld, J. H. *J. Phys. Chem.* **1996**, *100*, 10967−10980.

(42) Koch, R.; Knispel, R.; Elend, M.; Zetzsch, C. *Atmos. Chem. Phys. Discuss.* **2006**, *6*, 7623−7656. Bohn, B.; Zetzsch, C. *Phys. Chem. Chem. Phys.* **1999**, *1*, 5097−5107.

(43) Atkinson, R. *J. Phys. Chem. Ref. Data* **1991**, *20* (88), 459−507.

(44) Atkinson, R.; Plum, C. N.; Carter, W. P. L.; Winer, A. M.; Pitts, J. N., Jr. *J. Phys. Chem.* **1984**, *88*, 1210−1215. The values reported are $k \leq 1.1 \times 10^{-17}$ (benzene) and 6.4×10^{-15} s^{-1} cm^3 $molecules^{-1}$ (naphthalene).

(45) A test, carried out on **B-VI**, indicates that the hydroxyl addition to the unsaturated system is easier than H abstraction by 3.3 kcal mol^{-1} in terms of G. Reference 6 (Chapter 6, pp 182, 191, and 192) reports that HO carries a fast attack to the double CC bond ($k_{addition} \approx 10^{-11}-10^{-10}$ s^{-1} cm^3 $molecules^{-1}$), while the attack to an alkane is not as fast ($k_{abstraction} \approx 10^{-12}-10^{-11}$ s^{-1} cm^3 $molecules^{-1}$). A double bond in a conjugated diene is even more reactive (e.g., $k = 10^{-10}$ s^{-1} cm^3 $molecules^{-1}$ for isoprene).

(46) Rate constants for the reactions between alkyl peroxyl radicals and NO are collected in: Wallington, T. J.; Nielsen, O. J.; Sehested, J. Reactions of Organic Peroxy Radicals in the Gas Phase. In *Peroxyl Radicals*; Alfassi, Z. B., Ed.; Wiley: New York, 1997; Chapter 7. The values are all of the order of 10^{-12} cm^3 $molecule^{-1}$ s^{-1} (for instance, for $(CH_3)_2CH$-OO, $k = 3.5 \times 10^{-12}$ to 5×10^{-12} cm^3 $molecule^{-1}$ s^{-1}).

(47) See for instance: Jensen, F. *Computational Chemistry*; Wiley: New York, 1999; Section 12.3, in particular pp 306−307.

(48) Atkinson, R.; Arey, J.; Zielinska, B.; Aschmann, S. M. *Int. J. Chem. Kin.* **1990**, *21*, 999−1014.